analytical chemistry

Article

Cite This: Anal. Chem. XXXX, XXX, XXX−XXX

pubs.acs.org/ac

Flow Injection−Traveling-Wave Ion Mobility−Mass Spectrometry for Prostate-Cancer Metabolomics

Xiaoling Zang,[†] María Eugenia Monge,[‡] David A. Gaul,[†] and Facundo M. Fernández*[,†]

[†]School of Chemistry and Biochemistry, Georgia Institute of Technology, Atlanta, Georgia 30332, United States

[‡]Centro de Investigaciones en Bionanociencias (CIBION), Consejo Nacional de Investigaciones Científicas y Técnicas (CONICET), Godoy Cruz 2390, Ciudad de Buenos Aires C1425FQD, Argentina

Supporting Information

ABSTRACT: Flow injection−traveling-wave ion mobility−mass spectrometry (FI-TWIM-MS) was applied to the nontargeted metabolic profiling of serum extracts from 61 prostate-cancer (PCa) patients and 42 controls with an analysis speed of 6 min per sample, including a 3 min wash run. Comprehensive data mining of the mobility−mass domain was used to discriminate species with various charge states and filter matrix salt-cluster ions. Specific criteria were developed to ensure correct grouping of adducts, in-source fragments, and impurities in the data set. Endogenous metabolites were identified with high confidence using FI-TWIM-MS/MS and collision-cross-section (CCS) matching with chemical standards or CCS databases. PCa patient samples were distinguished from control samples with good accuracies (88.3−89.3%), sensitivities (88.5−90.2%), and specificity (88.1%) using supervised multivariate classification methods. Although largely underutilized in metabolomics studies, FI-TWIM-MS proved advantageous in terms of analysis speed, separation of ions in complex mixtures, improved signal-to-noise ratio, and reduction of spectral congestion. Results from this study showcase the potential of FI-TWIM-MS as a high-throughput metabolic-profiling tool for large-scale metabolomics studies.

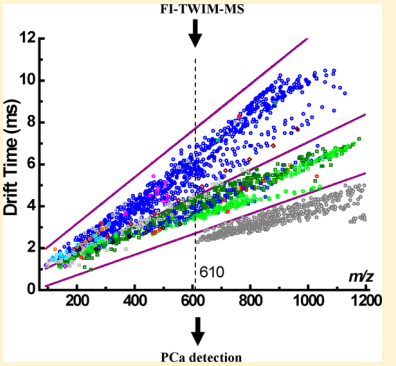

Metabolomics has emerged as a powerful tool to better understand biochemical processes and discover potential disease biomarkers, thereby improving diagnosis, prognosis, and monitoring of disease progression.[1−4] Mass spectrometry (MS) and nuclear magnetic resonance (NMR) are the most commonly used analytical platforms in metabolomics, with NMR providing better structural information and MS yielding wider metabolome coverage because of its higher sensitivity. Coupling of liquid chromatography to MS (LC-MS) adds an orthogonal axis to mass-to-charge-ratio (m/z) separations, thereby helping with metabolite identification in nontargeted studies and lessening the extent of ion suppression in complex matrices.

Identification of biological alterations in human metabolomes is often confounded by the inherent biological variance within patient cohorts. The most powerful strategy to overcome this challenge involves increasing cohort sizes to yield hundreds or even thousands of patient-derived samples, leading to the discovery of more robust metabolic signatures.[5,6] Increasing cohort size, however, necessarily comes at the expense of higher study costs and increased instrument-time demands. In most studies, most of that instrument time is typically consumed by the front-end LC separation.

Flow injection (FI) or direct infusion (DI) MS, without LC, maximize analytical throughput and eliminate problems of retention-time shifts due to column aging;[7,8] therefore, they are well-suited to larger patient cohorts. In a standard LC-MS system, the sample can be introduced to the mobile-phase flow for MS analysis using the flow injection method or directly introduced to the mass spectrometer by an external pump using the direct infusion method. Compared with DI-MS, FI-MS can be more easily automated on standard LC-MS instruments, with the added advantage of reducing the amount of sample required for analysis. Furthermore, addition of a post-ionization ion-mobility (IM) dimension to FI-MS provides rapid separation of gas-phase ions on the basis of collision-cross-section (CCS) differences.[9,10] Compared with FI-MS alone, the inclusion of such an IM dimension (i) reduces spectral overlap by separating compounds with different charge states and structural motifs that are distributed into distinct regions on the mobility−mass plot, (ii) increases signal-to-noise ratios, (iii) increases peak capacities, (iv) enables obtaining CCS values that provide an additional molecular descriptor useful in assigning chemical structures,[11] and (v) provides cleaner MS/MS spectra by avoiding precursor-ion coselection while still maintaining high analysis speed.[12,13] DI-IM-MS and FI-IM-MS, however, still remain largely underutilized in metabolomics, with the former applied only in a handful of studies without full exploitation of MS/MS or CCS information for metabolite identification.[14−16]

Prostate cancer (PCa) is the second leading cause of cancer-related mortality in American men, with 29 430 estimated

Received: September 18, 2018
Accepted: October 31, 2018
Published: October 31, 2018

DOI: 10.1021/acs.analchem.8b04259
Anal. Chem. XXXX, XXX, XXX−XXX

deaths in the United States in 2018.[17] The current PCa-screening approach includes the prostate-specific antigen (PSA) blood test and digital rectal examination (DRE). However, the PSA test suffers from overdiagnosis and overtreatment, and the DRE is limited by its low detection rate in cases where PCa presents nonpalpable growths.[18,19] Consequently, there has been a constant drive to discover new PCa biomarkers to improve or replace existing ones.[20] Along these lines, metabolomics studies have reported potential PCa biomarker panels that include amino acids,[21−26] organic acids,[23,27,28] polyamines,[27,28] lipids,[23,29,30] and carbohydrates,[22,31] with the majority of these studies employing the more time-consuming LC-MS and gas-chromatography (GC) MS approaches.[20,32] In this work, we demonstrate that FI-IM-MS produces data that is comparable to LC-MS in terms of PCa classification power, with the added advantage of higher sample throughput.

EXPERIMENTAL SECTION

Chemicals. Ultrapure water with 18.2 MΩ·cm resistivity (Barnstead Nanopure UV ultrapure water system), Optima LC-MS-grade acetonitrile and methanol (Fisher Scientific), and Omnisolv high-purity dichloromethane and HPLC-grade acetone (EMD) were used for mobile-phase preparation, sample preparation, and chemical-standard-solution preparation. LC-MS-grade acetic acid, uric acid (≥99%), nonanedioic acid (azelaic acid, 98%), tryptophan, inosine (≥99%), glutamine, histidine, leucine, isoleucine, L-allo-isoleucine, L-lysine (≥98%), uridine (≥99%), guanosine (≥98%), taurine (≥99%), indole (≥99%), phenylalanine, *m*-cresol (99%), *p*-cresol (99%), *o*-cresol, and sodium cholesterol sulfate were purchased from Sigma-Aldrich Corporation. Phenylalanyl phenylalanine was purchased from MP Biomedicals. Phenylacetylglutamine was purchased from Bachem. Lysophosphatidylcholine (LPC(18:0/0:0), 1-stearoyl-2-hydroxy-*sn*-glycerol-3-phosphocholine) was purchased from Avanti Polar Lipids Inc.

Cohort Description. Age-matched blood-serum samples were obtained from 61 PCa patients (age range 49−65, mean (SD) age 59(4) years) and 42 controls (age range 45−76, mean age 58(7) years). At the 0.05 level, the population age means were not significantly different according to the two-sample *t*-test. The cohort ethnicity was as follows: 21 African American (20.4%); 72 Caucasian (69.9%); 5 Hispanic (4.9%); 2 Asian (1.9%); 2 Jewish ancestry (1.9%); and 1 unknown (1.0%). After approval by the Institutional Review Board (IRB), blood samples were collected at Saint Joseph's Hospital of Atlanta, GA, by venipuncture from each donor into evacuated blood-collection tubes that contained no anticoagulant. Serum was obtained by centrifugation at 5000 rpm for 5 min at 4 °C. Immediately after centrifugation, 200 μL aliquots of serum were frozen and stored at −80 °C for further use. The sample collection and storage procedures for PCa patients and controls were identical.

Sample Preparation. Frozen serum samples were thawed on ice, and 300 μL of extraction solution (1:1:1 acetone/acetonitrile/methanol, cooled to −20 °C) was added to 100 μL of serum. Samples were vortex-mixed for 20 s and centrifuged at 16 000*g* for 5 min to pellet proteins. To remove most lipids and other nonpolar metabolites, 800 μL of dichloromethane was added to 350 μL of supernatant and vortex-mixed. Following the addition of 250 μL of deionized water, samples were vortex-mixed and kept on ice for 10 min. The aqueous phase was subject to flow injection−traveling-wave ion mobility−mass spectrometry (FI-TWIM-MS) analysis. Sample blanks were prepared using deionized water instead of serum following the same procedure.

FI-TWIM-MS and FI-TWIM-MS/MS Analysis Methods. FI-TWIM-MS metabolomic analysis was performed on a Waters ACQUITY UPLC I-Class system fitted with a stainless-steel union to bypass the column, which was coupled to a Synapt G2-S high-definition-mass-spectrometry (HDMS) system (Waters Corporation) operated in negative-ion mode. Major instrument settings were a capillary voltage of 2.2 kV, a cone voltage of 45 V, a source temperature of 120 °C, a desolvation-gas temperature of 300 °C, a desolvation-gas flow rate of 600 L h^{-1}, a helium-cell-gas flow rate of 180 mL min^{-1} and an IMS gas (N_2) flow rate of 90 mL min^{-1}. Mass spectra were acquired over the m/z range of 50−1200. For FI-TWIM-MS/MS experiments, precursor ions were fragmented in the transfer cell with ultrahigh-purity argon (≥99.999%) as the collision gas. Details on TWIM-, MS-, and MS/MS-measurement methods are provided in the Supporting Information.

Dt Measurement and CCS Calculations. For CCS-calibration purposes, a poly-DL-alanine solution was used as reference in negative-ion mode (10 mg L^{-1} in 50:50, v/v, acetonitrile/water). Calibration was performed using singly charged oligomers from n = 3 to 14, covering a mass range from 230 to 1012 Da and a CCS range from 150 to 308 $Å^2$. CCS values were derived using previously described procedures.[33] In MS/MS mode, Dt values were smaller because of the elevated collision voltage applied to the transfer cell, leading to increased speed of the ions traversing that chamber. In order to correct for this shift, CCS calibration was performed at each elevated collision voltage applied to the transfer cell in MS/MS experiments. CCS values for precursor ions in both MS and MS/MS modes were derived and compared well within 2% tolerance.

RESULTS AND DISCUSSION

A previous serum-metabolomics study from our group[23] showed feasibility of PCa detection using UPLC-MS on samples from the same cohort used in the present study, with each sample and wash run taking 18 and 8 min, respectively. In this study, FI-TWIM-MS was investigated as a new approach for metabolic fingerprinting with an analysis speed of 3 min for each sample run, followed by a 3 min wash run. A typical FI-TWIM-MS profile of a serum extract from a PCa patient is shown in Figure 1. The total-ion chronogram reached a

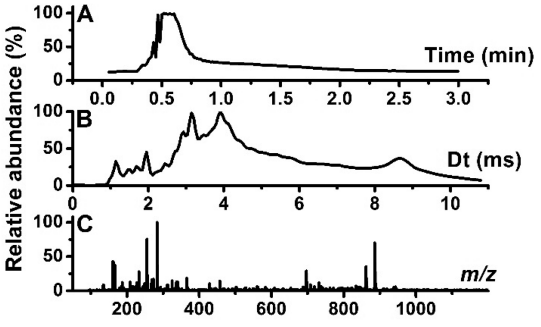

Figure 1. (A) Typical FI total-ion chronogram, (B) TWIM total-ion chronogram, and (C) combined mass spectrum of a serum extract from a PCa patient.

DOI: 10.1021/acs.analchem.8b04259
Anal. Chem. XXXX, XXX, XXX−XXX

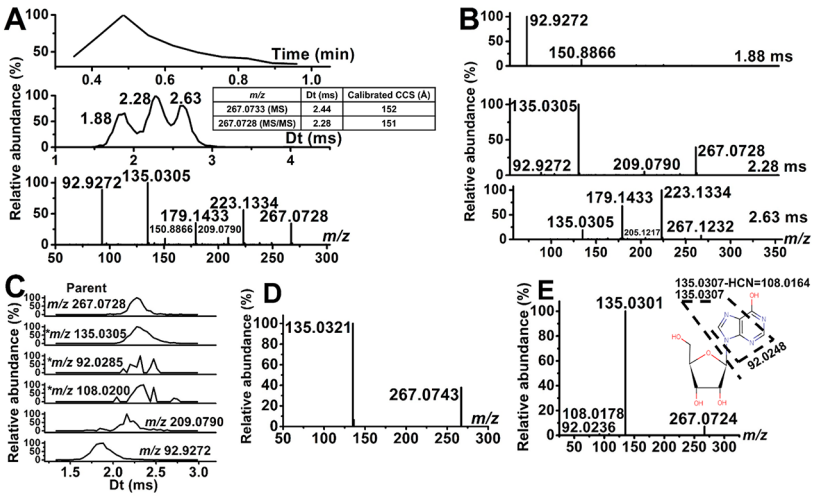

Figure 2. (A) FI-TWIM-MS/MS results for a PCa-serum-extract-sample feature detected in MS mode with m/z 267.0734 and Dt = 2.39 ms. Typical FI chronogram (top plot), TWIM total-ion chronogram (middle plot, with inset showing calibrated CCS values of precursor ions detected in both MS and MS/MS modes), and the corresponding total MS/MS spectrum (bottom plot). Tandem MS data were acquired by applying 25 V to the transfer cell. Small drift-time differences were observed between MS and MS/MS modes due to elevated bias voltage in the transfer cell when performing fragmentation experiments. (B) Extracted MS/MS spectra derived at Dt = 1.88, 2.28, and 2.63 ms. (C) TWIM extracted-ion chronograms for fragment ions with a mass tolerance of 10 mDa. Product-ion peaks aligned with the precursor ion at m/z 267.0734 are labeled with asterisks. (D) Inosine-standard MS/MS spectrum obtained in negative-ion mode using 25 V in the transfer cell. The observed Dt and CCS for this standard were 2.44 ms and 152 A^2, respectively. (E) Metlin MS/MS spectrum for inosine obtained in negative-ion mode with a collision-cell voltage of 20 V. All product ions were matched within a 4 mDa error.

maximum signal after ~0.5 min with analytes appearing within ~1 min after injection and began to tail off slowly as compounds dispersed in the flow system (Figure 1A). Figure 1B shows the corresponding TWIM total-ion chronogram that, as expected, indicates the presence of ionic species with a variety of shapes and charge states exhibiting drift times in the 1−10 ms range. The combined mass spectrum corresponding to the data in Figure 1A,B is shown in Figure 1C. These raw data were cleaned up by stringent data-processing methods to filter out unwanted features and group-redundant ionic species. The number of species remaining after each major step in the data-processing and -analysis workflow is shown in Table S1.

Compound Identification and Validation. After applying different filters and normalizing the data sets, features were searched in the HMDB,[34] and only those with tentative endogenous identities based on accurate-mass matching were retained (Figure S1). The remaining species were identified by matching CCS values and tandem MS spectra to databases, and whenever possible, their identity was validated by comparing Dt, CCS, and FI-TWIM-MS/MS spectra with chemical standards. An example of the identification workflow is illustrated in Figure 2 for a feature with m/z 267.0734 and Dt = 2.39 ms. Figure 2A shows the FI total-ion chronogram of a PCa-serum sample when performing MS/MS experiments (top panel), the associated TWIM total-ion chronogram (middle panel), and the corresponding combined MS/MS spectrum (bottom panel) extracted across Dt = 1.5−3 ms. Each of the three peaks identified in the TWIM total-ion chronogram with drift times of 1.88, 2.28, and 2.63 ms provided different MS/MS spectra (Figure 2B). Following CCS calibration, only the precursor ion extracted from the MS/MS mobility species with Dt = 2.28 ms matched the CCS of the feature of interest (m/z 267.0734) observed in the MS run (Figure 2A, middle panel inset) with an error of −0.66%. This species yielded the MS/MS spectrum shown in Figure 2B (middle panel). To further confirm that the species detected in Figure 2B (middle) corresponded to the precursor of interest, fragment-ion drift times were matched with that of the precursor ion. Figure 2C shows that only three out of the five fragment ions observed in the MS/MS spectrum of Figure 2B (middle panel) were actually product ions that aligned with the Dt of the precursor ion of interest. Further analysis of the spectral data indicated that the species at m/z 92.9272, identified as $[NaCl_2]^-$, was a fragment ion of the cluster $[Na_4Cl_5]^-$ with Dt = 1.88 ms and m/z 266.8039 (Figure S2), which partially overlapped with the species at Dt = 2.28 ms in the TWIM chronogram (Figure 2A, middle). Accurate-mass-based search in the HMDB[34] suggested inosine as the most likely candidate for this compound. Its tentative identity was confirmed by matching the experimental MS/MS spectrum with that of an inosine chemical standard (Figure 2D) and by comparing the MS/MS spectrum in the Metlin database[35] (Figure 2E). Further validation of this metabolite's identity was achieved by matching the MS-mode Dt and CCS with those of an inosine chemical standard and literature CCS values.[9] Similar procedures were applied to the identification of all compounds retained following the application of data filters (Tables 1 and S2).

Distribution of Compounds in the Mobility−Mass Plot. The distribution of different classes of ionic species present in the FI-TWIM-MS data set is shown in a mobility−mass plot (Figure 3), with each symbol representing an ionic compound with a specific pair of Dt and m/z values. Ionic species were distributed across three distinct regions separated by linear boundaries. The first area consisted mostly of singly charged compounds, including identified polar and lipid metabolites, dicarboxylic acids and their corresponding monoesters, and sodium acetate clusters. Features with high mass defects as defined by the McMillan filter[36] lay between the first and second plot regions. The second plot area consisted mostly of doubly charged compounds, together with some singly charged sodium chloride cluster ions and very few

DOI: 10.1021/acs.analchem.8b04259
Anal. Chem. XXXX, XXX, XXX−XXX

Table 1. Chemical Identities of Compounds Involved in the oPLS-DA Models

model	compound code	experimental m/z	Dt (ms)	most-abundant ion type	elemental formula	Δm (mDa)	tentative metabolite identity	mean fold change (PCa vs control)		p-value[a]		metabolite ID validation	CCS (Å^2) (percent error from database, percent error from standard)
								panel A	panel B	panel A	panel B		
A, B	**1**	311.1401	3.15	$[M-H]^-$	$C_{18}H_{20}N_2O_3$	0.0	phenylalanyl phenylalanine (phe−phe)	−1.9	−2.1	**9.1×10^{-5}**	**4.4×10^{-5}**	Dt, MS/MS[b,e]	175 (N/A, 0)
A, B	**2**	203.0848	2.17	$[M-H]^-$	$C_{11}H_{12}N_2O_2$	2.2	tryptophan	−1.1	−1.1	0.21	0.040	Dt, MS/MS[b,c,e]	145 (−0.68, 0)
B	**3**	116.0500	1.55	$[M-H]^-$	C_8H_7N	−0.6	indole	1.2	1.1		0.21	Dt[e]	126 (N/A, 0.81)
A, B	**4**	167.0214	1.52	$[M-H]^-$	$C_5H_4N_4O_3$	0.3	uric acid	1.3	1.2	**5.2×10^{-9}**	**8.0×10^{-6}**	Dt, MS/MS[b,c,e]	120 (−2.4, 0)
B	**5**	187.0075	1.79	$[M-H]^-$	$C_7H_8O_4S$	0.5	*p*-cresol sulfate	−1.0	−1.1		0.86	Dt, MS/MS[b,c,e] for in-source fragment *p*-cresol	131 for 187.0075, 122 for 107.0495 (in-source fragment of *p*-cresol) (N/A, 1.66)
A, B	**6**	476.2769	4.56	$[M-H]^-$	$C_{23}H_{44}NO_7P$	−1.3	lysophosphatidyl ethanolamine (LPE(0:0/18:2), LPE(18:2/0:0))	1.2	1.2	0.23	0.48	MS/MS[c]	213 (N/A, N/A)
A, B	**7**	263.1052	2.60	$[M-H]^-$	$C_{13}H_{16}N_2O_4$	1.5	phenylacetyl glutamine	−2.0	−2.1	0.0094	**0.0029**	Dt, MS/MS[c,e]	158 (N/A, −1.3)
B	**8**	145.0975	1.74	$[M-H]^-$	$C_6H_{14}N_2O_2$	−0.8	lysine		−1.0		0.44	Dt[e]	131 (−1.5, −1.5)
A, B	**9**	504.3095	4.94	$[M-CH_3]^-$	$C_{26}H_{50}NO_7P$	0.0	LPC(18:2/0:0), LPC(0:0/18:2)	−1.0	−1.1	0.67	0.30	MS/MS[c]	222 (N/A, N/A)
B	**10**	130.0857	1.68	$[M-H]^-$	$C_6H_{13}NO_2$	−1.7	leucine, isoleucine, allo-isoleucine		1.2		0.053	Dt[e]	130 (0.78, 0)
A	**11**	508.3423	5.13	$[M-CH_3]^-$	$C_{26}H_{54}NO_7P$	1.5	LPC(18:0/0:0), LPC(0:0/18:0)	1.1		0.042		Dt, MS/MS[c,e] for LPC(18:0/0:0)	227 (N/A, 0 for LPC(18:0/0:0))
A	**12**	369.1729	3.69	$[M-H]^-$	$C_{19}H_{30}O_5S$	−1.2	androsterone sulfate, 5α-dihydrotestosterone sulfate	1.2		0.11		MS/MS[b,c]	190 (N/A, N/A)
A	**13**	187.0971	1.90	$[M-H]^-$	$C_9H_{16}O_4$	−0.5	nonanedioic acid (azelaic acid)	−2.0		**2.8×10^{-11}**		Dt, MS/MS[b,c,e]	135 (N/A, 0)
A	**14**	273.1711	2.71	$[M-H]^-$	$C_{14}H_{26}O_5$	0.4	azelaic acid monohydroxypentyl ester (major) and undecanedioic acid monohydroxypropyl ester	−1.3		**9.4×10^{-8}**		MS/MS[b] for both, MS/MS[d] for azelaic acid monohydroxypentyl ester	162 (N/A, N/A)
A	**15**	287.1863	2.88	$[M-H]^-$	$C_{15}H_{28}O_5$	0.0	sebacic acid monohydroxypentyl ester (major) and dodecanedioic acid monohydroxypropyl ester	−1.3		**2.5×10^{-4}**		MS/MS[c]	167 (N/A, N/A)

[a]p-values were calculated by Wilcoxon rank-sum test. Statistically significant fold changes with Bonferroni corrections are shown in bold. All identified compounds were accurate-mass- and isotopic-pattern-matched. [b]MS/MS matched the Metlin database; [c]MS/MS matched manual fragmentation analysis. [d]MS/MS matched literature evidence. [e]Dt or MS/MS matched chemical standard.

DOI: 10.1021/acs.analchem.8b04259
Anal. Chem. XXXX, XXX, XXX−XXX

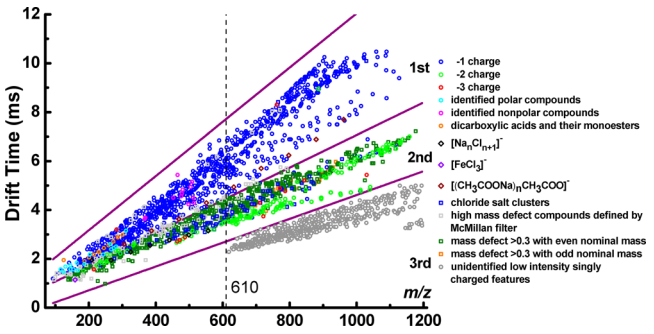

Figure 3. Mobility−mass plot for all ionic species detected in the FI-TWIMS-MS data set.

triply charged compounds. The third plot area contained unidentified, low-intensity, singly charged features with m/z > 600. Consequently, species in the second and third regions were removed from the data set.

The subset of features detected in the sample-preparation blanks included 9 different sodium acetate clusters; 229 chloride-salt-cluster ions; and 297 high-mass-defect features, of which 217 were chloride-salt-cluster ions (Figure S3). These composed 12.2% of the total detected features shown in Figure 3. Following blank filtering, a total of 1878 features were retained in the data set (Figure S4). A number of salt clusters still remained even after blank filtering, likely originating from the sample matrix.[36] Most of these salt clusters were removed by mass-defect filtering as a result of their high mass-defect m/z values.[36] Features retained following the application of all remaining filters are displayed in Figure S5, with all endogenous metabolites with identities confirmed by MS/MS or chemical standards shown in Figure S6. Less-stringent filtering approaches could also be applied to the data set, with the caveat that identification of the involved unknown compounds may be difficult or even impossible, thereby limiting the biological interpretation of the role of the metabolites involved in PCa pathogenesis.

Multivariate Analysis. Following data processing, the resulting data set was normalized by total ion intensity, yielding a data set named "dataset 1". A different data set (data set 2) was generated by total-ion-intensity normalization after the deletion of species identified as dicarboxylic acids and their monoesters, which might be of either endogenous or exogenous origin. After application of a prevalence filter, the identified compounds in data set 1 matching discriminant metabolites from our previous LC-MS PCa metabolomics study[23] were grouped into a new data set named "dataset A", and all identified endogenous metabolites in data set 2 were grouped into "dataset B". The final data sets consisting of 11 (dataset A) and 28 (dataset B) metabolites were subjected to supervised multivariate analysis. Two oPLS-DA models were built with these data sets using three-block cross-validation.

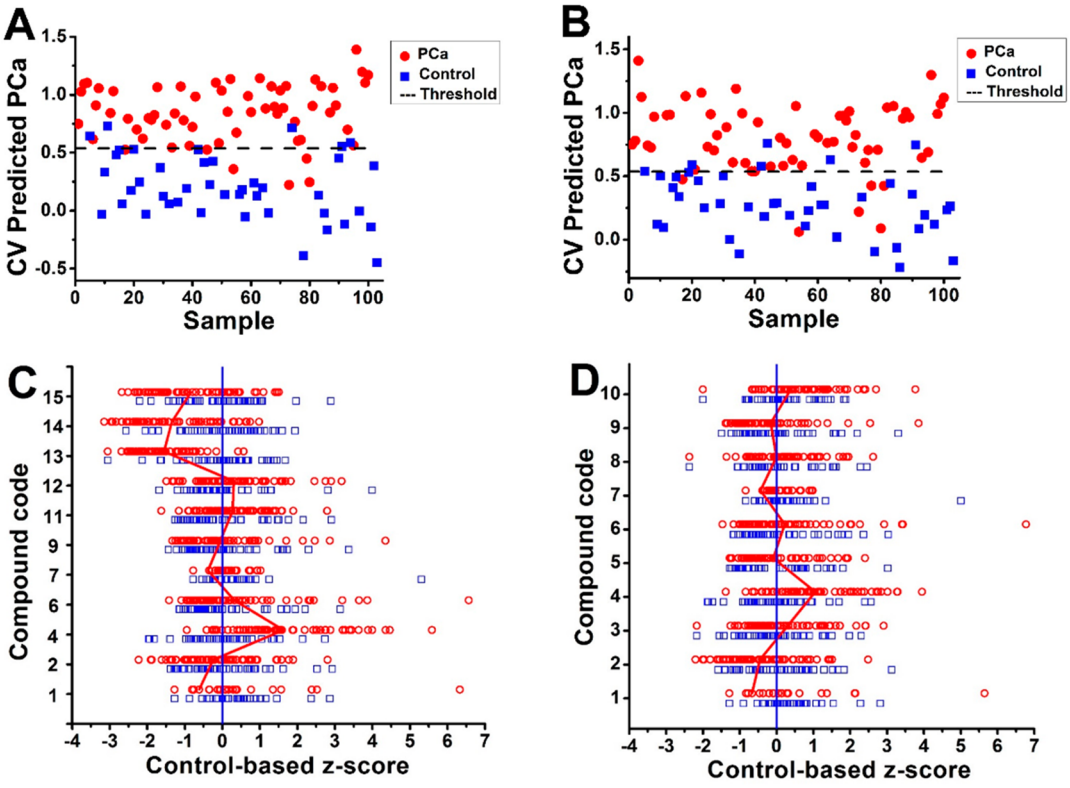

Figure 4. (A,B) oPLS-DA three-block cross-validated classification plots for models A and B, respectively. The x-axis represents sample number, and the y-axis represents the cross-validated scores predicted by the oPLS-DA classification model. PCa and control samples are represented by filled red circles and blue squares, respectively. The decision line for sample classification is represented by a black dashed line. (C,D) Control-based z-score plot of the 11 compounds in panel A and 10 discriminant compounds in panel B, respectively. PCa and control samples are represented by open red circles and blue squares, respectively. The z-scores were calculated as $(x - \mu)/\sigma$, where x is the normalized peak abundance of the compound in each sample, μ is the mean normalized peak abundance of the compound in the control samples, and σ is the standard deviation of the normalized peak abundance of the compound in the control samples. The red and blue lines at z-score = 0 connect the average z-scores of each compound in the PCa and control samples, respectively.

DOI: 10.1021/acs.analchem.8b04259
Anal. Chem. XXXX, XXX, XXX−XXX

The performance of such models is shown in Table S3. Model A yielded an overall classification accuracy of 89.3%, a sensitivity of 90.2%, and a specificity of 88.1% (Table S3 and Figure 4A). When PCA was performed on this data set, good unsupervised sample clustering was achieved according to class membership (Figure S7).

Azelaic acid, identified as a key differentiating metabolite in PCa detection in our previous LC-MS study,[23] can originate from both the free acid species or from in-source cleavage of its monoesters. Although distinguishable by chromatography (Figure S8), in FI-TWIMS-MS experiments all azelaic acid related species are simultaneously ionized to produce a single FI peak. Because azelaic acid and its esters might be of exogenous origin[37] along with a lack of a clear biological role, we tested removing the corresponding signals as well as signals for other dicarboxylic acids and their esters (Table S4) to see if a discriminant-metabolite panel could be obtained without their contribution.

A second oPLS-DA model (model B) was created using data set B. Out of the initial set of 28 metabolites, 10 were selected by iPLS-DA as being optimum, yielding a discriminant-metabolite panel with a maximum classification accuracy of 88.3%, a sensitivity of 88.5%, and a specificity of 88.1% (Table S3 and Figure 4B). Both models yielded Q^2 values (model predictive ability) larger than 0.5, and an area under the receiver-operating-characteristic curve (AUC) larger than 0.9. In addition, sample-label-permutation-test results suggested low probability of data overfitting, demonstrating the robustness of the oPLS-DA models and the reliability of both discriminant compound panels.

Table 1 details the identities of the compounds involved in each of the oPLS-DA models, together with the methods used for validation of their chemical identities. All compounds were identified within 2.5 mDa error for precursor ions, and 8 mDa for fragment ions in their MS/MS spectra. Experimental CCS values were matched within ±3% of database or chemical-standard values analyzed under identical conditions. Table S2 details the identities of the compounds not selected by iPLS-DA.

Univariate analysis was also performed for the discriminant compounds in panels A and B. Compounds that presented statistically significant fold changes with Bonferroni correction between PCa and control samples are indicated in Table 1. The *z*-score plots for discriminant compounds from panels A and B normalized to the mean abundances of the control samples are shown in Figure 4C,D, respectively. The discriminant compounds with significant changes between sample classes were univocally identified as uric acid (significant changes in both panels), phenylalanyl phenylalanine (significant changes in both panels), phenylacetyl glutamine (significant change in panel B), azelaic acid monohydroxy-pentyl ester and undecanedioic acid monohydroxy-propyl ester (panel A), and sebacic acid monohydroxy-pentyl ester and dodecanedioic acid monohydroxy-propyl ester (panel A). The fact that all compounds that were observed as being significantly altered in this study coincided with the discriminant-metabolite panel in our previous LC-MS study,[23] with identical fold-change directions between the PCa and control samples, corroborated the feasibility and accuracy of the FI-TWIM-MS method proposed here as providing a viable alternative to UPLC-MS.

Biological Roles of Discriminant Metabolites. Uric acid, with a significant positive fold change (Table 1) between PCa- and control-serum samples, has pro-inflammatory properties, and elevated serum uric acid (hyperuricemia) has been reported to be associated with increased cancer (including PCa) risk, recurrence, and mortality.[38,39] Tryptophan levels were decreased in PCa-patient samples compared with in the controls in panel B (Table 1). Consumption of tryptophan has been found to be a crucial factor in cancer progression,[40] and inhibition of tryptophan 2,3-dioxygenase, which degrades tryptophan in the kynurenine pathway, has been reported to reverse tumoral immune resistance in mice.[41] Interestingly, indole, which is a bacterial-degradation product of tryptophan, was also identified among the discriminant compounds in panel B with a small elevation in the average abundance in sera of PCa patients compared with in those of the controls (Table 1). LPC(18:0) has been reported to be one of the discriminant plasma lipids for PCa, with a significant increase in PCa patients compared with in the controls.[30] It is also slightly increased in PCa samples compared with in the controls in our study, although not significantly (Table 1). Azelaic acid, reported to be a potential antitumoral agent,[42] had a significant increase in the controls compared with in the PCa-patient samples in panel A, with the same trend observed for its corresponding monoesters (Table 1). However, the origin of azelaic acid and related monoesters warrants further investigation, as these species have also been reported as possibly originating from corn oil.[37]

Uniquely identified metabolites in data set 2 were input into Metaboanalyst[43] for pathway analysis, with several metabolic pathways with more than one metabolite hit indicated as significantly altered between PCa patients and controls ($p < 0.05$). These included purine metabolism, phenylalanine metabolism, aminoacyl-tRNA metabolism, and tryptophan metabolism (Figure S9). Elevated purine-nucleotide levels have been reported to be sufficient to induce major histocompatibility class I chain-related protein A (MICA) expression on abnormal or stressed cells, including cancer cells.[44] De novo purine biosynthesis has been suggested to support elevated transcription and cell-division levels in PCa cells and may provide a target for PCa treatment.[45] Phenylalanine and tyrosine restriction has been found to induce PCa cell death via glucose-metabolism modulation.[46] In addition, phenylalanine has also been reported to be significantly increased in PCa metastatic bone tissue compared with in normal bone in a nontargeted metabolomics study using GC-MS.[29] Aminoacyl-tRNA synthetases (AARSs) function as enzymes to catalyze the covalent linkage of amino acids to their corresponding tRNAs, and they play a crucial role in translation and cell signaling that is vital for cell function and viability.[47,48] AARSs have been suggested as potential therapeutic targets for cancer because of their cancer-related genetic profiles, mutations, and biological-pathway deregulations.[47,48] Metabolites involved in the tryptophan metabolic pathway have been found to be significantly altered in urine samples of PCa patients compared with in healthy controls.[49]

Limitations of the Proposed Approach. Despite the promise of the FI-TWIM-MS approach for rapid metabolomics fingerprinting, this technique is not without its limitations. Table S5 summarizes the strengths and limitations of FI-MS, FI-IM-MS, LC-MS, and LC-IM-MS according to several performance parameters. Clearly, a compromise between sample throughput and peak capacity is achieved in FI-IM-MS, with the lack of front-end LC separation being beneficial

DOI: 10.1021/acs.analchem.8b04259
Anal. Chem. XXXX, XXX, XXX−XXX

in terms of speed but detrimental in terms of differentiating intact ionic species from molecular compounds resulting from in-source fragmentation. Nevertheless, the power of FI-TWIM-MS resides in its speed and economy, rather than in its comprehensive separation power, as already discussed extensively.

CONCLUSION

In this study, we developed a fast FI-TWIM-MS serum-metabolic-profiling method for PCa detection, with an analysis speed of 3 min per sample, followed by a 3 min wash run. This overall time can likely be shortened by increasing the mobile-phase flow rate, optimizing the wash run, or replacing the current front-end FI system with a faster injection platform such as the RapidFire platform.[50] PCa-patient and control samples were distinguished with 88.3−89.3% accuracies, 88.5−90.2% sensitivities, and 88.1% specificity by using oPLS-DA classification. Discriminant metabolites were identified by matching accurate masses, CCS values, and fragmentation patterns in FI-TWIM-MS/MS to those in databases or to authentic chemical standards. CCS calibration was utilized to correct the ion drift-time shifts in TWIM-MS/MS experiments compared with those in TWIM-MS, greatly aiding in assigning the correct precursor ions. Stringent criteria were utilized for combining spectral features and grouping adduct ions, in-source fragments, and salt-cluster ions. Overall, our results indicated that FI-TWIM-MS is a promising tool that could be successfully applied to metabolic fingerprinting of large-scale cohorts, with its fast analysis speed and ion-separation capabilities being useful for interrogation of complex biological mixtures. Further improvements in sample throughput and development of an automated metabolite-identification pipeline should further increase the efficiency of the proposed metabolomics workflow.

ASSOCIATED CONTENT

Supporting Information

The Supporting Information is available free of charge on the ACS Publications website at DOI: 10.1021/acs.analchem.8b04259.

FI-TWIM-MS and FI-TWIM-MS/MS analysis methods; data-processing and -analysis workflow; number of ionic compounds retained after each major data-processing step; chemical identities of the compounds not selected by iPLS-DA; oPLS-DA-model classification performance; dicarboxylic acids and corresponding monoesters identified by negative-mode FI-TWIM-MS/MS; comparison of four popular MS-based techniques applied to nontargeted metabolomics; compound charge states found in various areas of mobility−mass plots; criteria applied for combining features, adduct ions, in-source fragment ions, and salt clusters in FI-TWIM-MS data; FI-TWIM-MS-metabolomics workflow used for data collection and analysis; example of the identification of $[Na_4Cl_5]^-$; mobility−mass plot of features detected in sample-preparation blanks, after the blank filter was applied, and after all filters were applied; mobility−mass plot of identified polar and lipid compounds grouped by classes in the final data set; PCA plot of all samples using normalized abundances of compounds; LC-TWIM-MS analysis of azelaic acid and its monoesters; and Metaboanalyst pathway analysis of uniquely identified metabolites in data set 2 (PDF)

AUTHOR INFORMATION

Corresponding Author

*E-mail: facundo.fernandez@chemistry.gatech.edu. Tel.: 404 385 4432. Fax: 404 385 6447.

ORCID

Xiaoling Zang: 0000-0002-2913-5799
María Eugenia Monge: 0000-0001-6517-5301
David A. Gaul: 0000-0002-9308-1895
Facundo M. Fernández: 0000-0002-0302-2534

Notes

The authors declare no competing financial interest.

ACKNOWLEDGMENTS

Drs. Nikhil Shah and Rajesh Laungani are acknowledged for sample collection at Saint Joseph's Hospital, Atlanta, GA. M.E.M. is a research staff member of the Consejo Nacional de Investigaciones Científicas y Técnicas (CONICET), Argentina.

REFERENCES

(1) Trivedi, D. K.; Hollywood, K. A.; Goodacre, R. *New Horiz. Transl. Med.* **2017**, *3*, 294−305.
(2) Armitage, E. G.; Barbas, C. *J. Pharm. Biomed. Anal.* **2014**, *87*, 1−11.
(3) Nagana Gowda, G. A.; Raftery, D. *Curr. Metabolomics* **2013**, *1*, 227−240.
(4) Kohler, I.; Hankemeier, T.; van der Graaf, P. H.; Knibbe, C. A. J.; van Hasselt, J. G. C. *Eur. J. Pharm. Sci.* **2017**, *109S*, S15−S21.
(5) Blaise, B. J.; Correia, G.; Tin, A.; Young, J. H.; Vergnaud, A. C.; Lewis, M.; Pearce, J. T.; Elliott, P.; Nicholson, J. K.; Holmes, E.; Ebbels, T. M. *Anal. Chem.* **2016**, *88*, 5179−5188.
(6) Krzywinski, M.; Altman, N. *Nat. Methods* **2013**, *10*, 1139−1140.
(7) Beckmann, M.; Parker, D.; Enot, D. P.; Duval, E.; Draper, J. *Nat. Protoc.* **2008**, *3*, 486−504.
(8) Gonzalez-Dominguez, R.; Sayago, A.; Fernandez-Recamales, A. *Bioanalysis* **2017**, *9*, 131−148.
(9) Paglia, G.; Williams, J. P.; Menikarachchi, L.; Thompson, J. W.; Tyldesley-Worster, R.; Halldorsson, S.; Rolfsson, O.; Moseley, A.; Grant, D.; Langridge, J.; Palsson, B. O.; Astarita, G. *Anal. Chem.* **2014**, *86*, 3985−3993.
(10) Paglia, G.; Angel, P.; Williams, J. P.; Richardson, K.; Olivos, H. J.; Thompson, J. W.; Menikarachchi, L.; Lai, S.; Walsh, C.; Moseley, A.; Plumb, R. S.; Grant, D. F.; Palsson, B. O.; Langridge, J.; Geromanos, S.; Astarita, G. *Anal. Chem.* **2015**, *87*, 1137−1144.
(11) Soper-Hopper, M. T.; Petrov, A. S.; Howard, J. N.; Yu, S. S.; Forsythe, J. G.; Grover, M. A.; Fernandez, F. M. *Chem. Commun. (Cambridge, U. K.)* **2017**, *53*, 7624−7627.
(12) Kurulugama, R. T.; Valentine, S. J.; Sowell, R. A.; Clemmer, D. E. *J. Proteomics* **2008**, *71*, 318−331.
(13) Paglia, G.; Astarita, G. *Nat. Protoc.* **2017**, *12*, 797−813.
(14) Dwivedi, P.; Wu, P.; Klopsch, S. J.; Puzon, G. J.; Xun, L.; Hill, H. H. *Metabolomics* **2008**, *4*, 63−80.
(15) Kaplan, K.; Dwivedi, P.; Davidson, S.; Yang, Q.; Tso, P.; Siems, W.; Hill, H. H. *Anal. Chem.* **2009**, *81*, 7944−7953.
(16) Isailovic, D.; Plasencia, M. D.; Gaye, M. M.; Stokes, S. T.; Kurulugama, R. T.; Pungpapong, V.; Zhang, M.; Kyselova, Z.; Goldman, R.; Mechref, Y.; Novotny, M. V.; Clemmer, D. E. *J. Proteome Res.* **2012**, *11*, 576−585.
(17) Siegel, R. L.; Miller, K. D.; Jemal, A. *Ca-Cancer J. Clin.* **2018**, *68*, 7−30.

DOI: 10.1021/acs.analchem.8b04259
Anal. Chem. XXXX, XXX, XXX−XXX

(18) Lee, F.; Littrup, P. J.; Torppedersen, S. T.; Mettlin, C.; McHugh, T. A.; Gray, J. M.; Kumasaka, G. H.; McLeary, R. D. *Radiology* **1988**, *168*, 389−394.
(19) Tombal, B. *Eur. Urol., Suppl.* **2006**, *5*, 511−513.
(20) Lima, A. R.; Bastos, M. d. L.; Carvalho, M.; Guedes de Pinho, P. *Transl. Oncol.* **2016**, *9*, 357−370.
(21) Miyagi, Y.; Higashiyama, M.; Gochi, A.; Akaike, M.; Ishikawa, T.; Miura, T.; Saruki, N.; Bando, E.; Kimura, H.; Imamura, F.; Moriyama, M.; Ikeda, I.; Chiba, A.; Oshita, F.; Imaizumi, A.; Yamamoto, H.; Miyano, H.; Horimoto, K.; Tochikubo, O.; Mitsushima, T.; et al. *PLoS One* **2011**, *6*, No. e24143.
(22) Struck-Lewicka, W.; Kordalewska, M.; Bujak, R.; Yumba Mpanga, A.; Markuszewski, M.; Jacyna, J.; Matuszewski, M.; Kaliszan, R.; Markuszewski, M. J. *J. Pharm. Biomed. Anal.* **2015**, *111*, 351−361.
(23) Zang, X. L.; Jones, C. M.; Long, T. Q.; Monge, M. E.; Zhou, M. S.; Walker, L. D.; Mezencev, R.; Gray, A.; McDonald, J. F.; Fernandez, F. M. *J. Proteome Res.* **2014**, *13*, 3444−3454.
(24) Shuster, J. R.; Lance, R. S.; Troyer, D. A. *BMC Clin. Pathol.* **2011**, *11*, 14.
(25) Brown, M. V.; McDunn, J. E.; Gunst, P. R.; Smith, E. M.; Milburn, M. V.; Troyer, D. A.; Lawton, K. A. *Genome Med.* **2012**, *4*, 33.
(26) Sreekumar, A.; Poisson, L. M.; Rajendiran, T. M.; Khan, A. P.; Cao, Q.; Yu, J.; Laxman, B.; Mehra, R.; Lonigro, R. J.; Li, Y.; Nyati, M. K.; Ahsan, A.; Kalyana-Sundaram, S.; Han, B.; Cao, X.; Byun, J.; Omenn, G. S.; Ghosh, D.; Pennathur, S.; Alexander, D. C.; et al. *Nature* **2009**, *457*, 910−914.
(27) Swanson, M. G.; Vigneron, D. B.; Tabatabai, Z. L.; Males, R. G.; Schmitt, L.; Carroll, P. R.; James, J. K.; Hurd, R. E.; Kurhanewicz, J. *Magn. Reson. Med.* **2003**, *50*, 944−954.
(28) Swanson, M. G.; Zektzer, A. S.; Tabatabai, Z. L.; Simko, J.; Jarso, S.; Keshari, K. R.; Schmitt, L.; Carroll, P. R.; Shinohara, K.; Vigneron, D. B.; Kurhanewicz, J. *Magn. Reson. Med.* **2006**, *55*, 1257−1264.
(29) Thysell, E.; Surowiec, I.; Hornberg, E.; Crnalic, S.; Widmark, A.; Johansson, A. I.; Stattin, P.; Bergh, A.; Moritz, T.; Antti, H.; Wikstrom, P. *PLoS One* **2010**, *5*, No. e14175.
(30) Zhou, X. C.; Mao, J. H.; Ai, J. M.; Deng, Y. P.; Roth, M. R.; Pound, C.; Henegar, J.; Welti, R.; Bigler, S. A. *PLoS One* **2012**, *7*, No. e48889.
(31) Wu, H.; Liu, T. T.; Ma, C. G.; Xue, R. Y.; Deng, C. H.; Zeng, H. Z.; Shen, X. Z. *Anal. Bioanal. Chem.* **2011**, *401*, 635−646.
(32) Kelly, R. S.; Vander Heiden, M. G.; Giovannucci, E.; Mucci, L. A. *Cancer Epidemiol., Biomarkers Prev.* **2016**, *25*, 887−906.
(33) Bush, M. F.; Campuzano, I. D. G.; Robinson, C. V. *Anal. Chem.* **2012**, *84*, 7124−7130.
(34) Wishart, D. S.; Jewison, T.; Guo, A. C.; Wilson, M.; Knox, C.; Liu, Y.; Djoumbou, Y.; Mandal, R.; Aziat, F.; Dong, E.; Bouatra, S.; Sinelnikov, I.; Arndt, D.; Xia, J.; Liu, P.; Yallou, F.; Bjorndahl, T.; Perez-Pineiro, R.; Eisner, R.; Allen, F.; et al. *Nucleic Acids Res.* **2013**, *41*, D801−D807.
(35) Smith, C. A.; O'Maille, G.; Want, E. J.; Qin, C.; Trauger, S. A.; Brandon, T. R.; Custodio, D. E.; Abagyan, R.; Siuzdak, G. *Ther. Drug Monit.* **2005**, *27*, 747−751.
(36) McMillan, A.; Renaud, J. B.; Gloor, G. B.; Reid, G.; Sumarah, M. W. *J. Cheminf.* **2016**, *8*, 44.
(37) Matsubara, T.; Tanaka, N.; Krausz, K. W.; Manna, S. K.; Kang, D. W.; Anderson, E. R.; Luecke, H.; Patterson, A. D.; Shah, Y. M.; Gonzalez, F. J. *Cell Metab.* **2012**, *16*, 634−644.
(38) Fini, M. A.; Elias, A.; Johnson, R. J.; Wright, R. M. *Clin. Trans. Med.* **2012**, *1*, 16.
(39) Kolonel, L. N.; Yoshizawa, C.; Nomura, A. M.; Stemmermann, G. N. *Cancer Epidemiol. Biomarkers Prev.* **1994**, *3*, 225−228.
(40) Prendergast, G. C. *Nature* **2011**, *478*, 192−194.
(41) Pilotte, L.; Larrieu, P.; Stroobant, V.; Colau, D.; Dolusic, E.; Frederick, R.; De Plaen, E.; Uyttenhove, C.; Wouters, J.; Masereel, B.; Van den Eynde, B. J. *Proc. Natl. Acad. Sci. U. S. A.* **2012**, *109*, 2497−2502.
(42) Breathnach, A. S. *Med. Hypotheses* **1999**, *52*, 221−226.
(43) Xia, J. G.; Sinelnikov, I. V.; Han, B.; Wishart, D. S. *Nucleic Acids Res.* **2015**, *43*, W251−W257.
(44) McCarthy, M. T.; Moncayo, G.; Hiron, T. K.; Jakobsen, N. A.; Valli, A.; Soga, T.; Adam, J.; O'Callaghan, C. A. *J. Biol. Chem.* **2018**, *293*, 3913−3924.
(45) Barfeld, S. J.; Fazli, L.; Persson, M.; Marjavaara, L.; Urbanucci, A.; Kaukoniemi, K. M.; Rennie, P. S.; Ceder, Y.; Chabes, A.; Visakorpi, T.; Mills, I. G. *Oncotarget* **2015**, *6*, 12587−12602.
(46) Fu, Y. M.; Lin, H. M.; Liu, X. Y.; Fang, W. G.; Meadows, G. G. *J. Cell. Physiol.* **2010**, *224*, 491−500.
(47) Kim, S.; You, S.; Hwang, D. *Nat. Rev. Cancer* **2011**, *11*, 708−718.
(48) Rajendran, V.; Kalita, P.; Shukla, H.; Kumar, A.; Tripathi, T. *Int. J. Biol. Macromol.* **2018**, *111*, 400−414.
(49) Fernandez-Peralbo, M. A.; Gomez-Gomez, E.; Calderon-Santiago, M.; Carrasco-Valiente, J.; Ruiz-Garcia, J.; Requena-Tapia, M. J.; Luque de Castro, M. D.; Priego-Capote, F. *Sci. Rep.* **2016**, *6*, No. 38243.
(50) Zhang, X.; Romm, M.; Zheng, X.; Zink, E. M.; Kim, Y. M.; Burnum-Johnson, K. E.; Orton, D. J.; Apffel, A.; Ibrahim, Y. M.; Monroe, M. E.; Moore, R. J.; Smith, J. N.; Ma, J.; Renslow, R. S.; Thomas, D. G.; Blackwell, A. E.; Swinford, G.; Sausen, J.; Kurulugama, R. T.; Eno, N.; et al. *Clin. Mass Spectrom.* **2016**, *2*, 1−10.

DOI: 10.1021/acs.analchem.8b04259
Anal. Chem. XXXX, XXX, XXX−XXX